

## MAPPER-TYPE ALGORITHMS FOR COMPLEX DATA AND RELATIONS

PAWEŁ DŁOTKO<sup>1</sup>, DAVIDE GURNARI<sup>1</sup> AND RADMILA SAZDANOVIC<sup>1,2</sup>

**ABSTRACT.** Mapper and Ball Mapper are Topological Data Analysis tools used for exploring high dimensional point clouds and visualizing scalar-valued functions on those point clouds. Inspired by open questions in knot theory, new features are added to Ball Mapper that enable encoding of the structure, internal relations and symmetries of the point cloud. Moreover, the strengths of Mapper and Ball Mapper constructions are combined to create a tool for comparing high dimensional data descriptors of a single dataset. This new hybrid algorithm, Mapper on Ball Mapper, is applicable to high dimensional lens functions. As a proof of concept we include applications to knot and game theory, as well as material science and cancer research.

## 1. INTRODUCTION

Mapper [38] and Ball Mapper [33] algorithms are Topological Data Analysis (TDA) tools for exploring and visualizing data. The Mapper algorithm was introduced in 2007 and since then it has been used in a number of different applications, most notably medical data analysis [31], [23] and material science [41]. Ball Mapper [33] was introduced in 2019 as an easy-to-use effective alternative to the Mapper algorithm, see applications to data in economics [34].

Both techniques take a point cloud  $X$ , possibly with a scalar-valued function  $f : X \rightarrow \mathbb{R}$ , as an input, and return an abstract graph  $G = (V, E)$ , with a induced function  $\hat{f} : V \rightarrow \mathbb{R}$ . The "layout" of  $G$  resembles the multidimensional layout of the input set  $X$ . In addition, visualising  $\hat{f}$  over the vertices of  $G$ , typically using an appropriate color scale, provides insights into properties of the input function  $f$ . One of the first and most famous examples, further analyzed in this paper, is the work in [31], where the input point cloud consists of gene expression data for breast cancer patients, and the function  $f$  determine the survival rate. Mapper associated rare cancer with subtypes with 100% survival rate and allowed the authors to characterize its genetic profile.

This research introduces novel techniques that broaden and improve the scope and applicability of mapper-type algorithms to utilize additional structure of data and visualize the maps between datasets. Main contributions include:

- (1) *Equivariant Ball Mapper EqBM*: the most natural choice of mapper-type algorithms when the input data admits an action of a group of isometries or distance preserving bijection. The structure of the resulting Ball Mapper graph reflects the action of the input isometries.
- (2) *MappingMappers*: Mapper and Ball Mapper-based representations of high dimensional datasets  $X$  and  $Y$  can be used to visualize a given relation  $f : X \rightarrow Y$ . For example, if  $X$  and  $Y$  are values of different descriptors of the object of interest, such as different knots, materials, or cancer patients. MappingMappers can be used to compare descriptors' relevance and discover potential correlations or dependencies.

<sup>1</sup>DIOSCURI CENTRE IN TOPOLOGICAL DATA ANALYSIS, MATHEMATICAL INSTITUTE PAN, WARSAW, PL

<sup>2</sup>DEPARTMENT OF MATHEMATICS, NORTH CAROLINA STATE UNIVERSITY, RALEIGH, NC

*E-mail address:* pdlotko@impan.pl, dgurnari@impan.pl, rsazdanovic@math.ncsu.edu.

*Date:* March 29, 2023.

PD and DG acknowledge support by Dioscuri program initiated by the Max Planck Society, jointly managed with the National Science Centre (Poland), and mutually funded by the Polish Ministry of Science and Higher Education and the German Federal Ministry of Education and Research. RS is partially supported by NSF grant DMS-1854705.

- (3) *Mapper on Ball Mapper MoBM*: Extension of the Mapper algorithm that allows the use of high dimensional lens functions  $f : X \rightarrow \mathbb{R}^n$ , with  $n \gg 1$ . In the proposed technique, a Ball Mapper graph of the range of  $f$  is built to obtain an *adaptive cover* which is then used to construct the final Mapper graph.

The main running and motivating example in this paper is an analysis of data coming from knot theory which has recently opened up to big data techniques such as machine learning [17, 19, 40, 22, 8]. Knot theory point clouds created from polynomial knot invariants such as the Alexander, Jones and HOMFLYPT, are perfect for showcasing the strengths of the Equivariant, MappingMappers and Mapper on Ball Mapper algorithms. Additional examples related to game theory material science and cancer research are discussed to highlight the presented algorithms. however the detailed interpretations, as well as in depth analysis of knot theory results, are omitted as they do not fit in the scope of this paper.

Techniques developed in this work are accompanied with sample public-domain implementations and have wide applicability in different areas of science. The software implementing the discussed techniques and the interactive visualizations of all the plots in this paper are available at the webpage <https://dioscuri-tda.org/BallMapperKnots.html> and in [10].

The paper is organized as follows. Section 2 provides the necessary background on the Mapper and Ball Mapper algorithms. Section 3 focuses on adaptations and new developments of Mapper algorithms that are applicable to any point cloud. In Section 3.1 we develop a version of Ball Mapper that takes into account symmetries (global or partial) of the data. Section 3.2 describes a way to construct Mapper graphs for lens functions with high dimensional domains and codomains. In Section 3.3 we discuss how to combine the strengths of the Mapper and Ball Mapper algorithms to analyze data, relations between high dimensional point clouds, and visualize maps between different datasets. Section 4.1 provides informal minimal background information about relevant knot invariants while Section 4.2 describes a way to turn knot invariants into point clouds so they can be analyzed by TDA techniques. Section 4.3 present the results of application of the the presented Mapper-type techniques to the space of knots and their invariants, while Section 4.4 focuses on the comparison of knot invariants using techniques from Section 3.3 and shows how the presented technique can benefit theoretical mathematics. Finally, Section 5 provides additional examples of the use of the proposed techniques in game theory, materials science, and cancer research.

## 2. BACKGROUND

In this section we present the Mapper algorithm [38], a standard tool of Topological Data Analysis, as well as the recently developed Ball Mapper [33].

**2.1. Mapper.** The *Mapper algorithm*, introduced in 2007 in [38], is one of the most recognizable tools of Topological Data Analysis. It can be considered a discrete approximation of a *Reeb graph* [36, 29]. An input for Mapper is a collection of points  $X$ , typically embedded in some high dimensional space, and a function  $f : X \rightarrow \mathbb{R}^n$ , referred to as the *lens function*. Typically, the range of the lens function is 1-dimensional. Next, construct the cover of the range  $f(X) \subset \mathbb{R}^n$  by a *collection of overlapping cubes of intervals*  $\mathcal{C}$ . For  $n = 1$ ,  $\mathcal{C}$  usually consists of  $k$  intervals covering  $f(X)$  such that two constitutive intervals overlap on  $p$  percent of their length. The number of intervals ( $k$ ) and the overlapping percentage ( $p$ ), often refereed to as *resolution* and *gain*, are additional input parameters of the Mapper algorithm.

For each element  $I \in \mathcal{C}$ , consider  $f^{-1}(I) \subset X$  and search for the clusters therein. The clustering algorithm used for that purpose is yet another parameter of the Mapper construction. For  $I \in \mathcal{C}$  let  $C_I$  indicate the collection of clusters found in  $f^{-1}(I)$ . Each cluster in  $\bigcup_{I \in \mathcal{C}} C_I$  corresponds to a vertex of an abstract graph  $G = (V, E)$ . Given a cluster  $A \in C_I$ , the vertex corresponding to

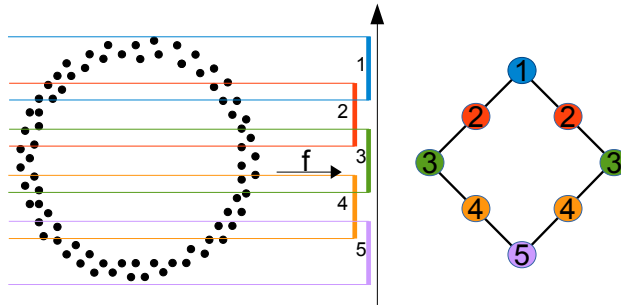


FIGURE 1. The Mapper construction illustration. The input is the 2-dimensional point cloud  $X$  in a shape of a circle shown on the left. The function  $f : X \rightarrow \mathbb{R}^1$  is a projection of a point to its second coordinate. We cover the range of  $f$  with five intervals, enumerated from 1 to 5, then compute the inverse image of each interval. In this example, the inverse images of intervals 1 and 5 contain one cluster, while inverse images of intervals 2, 3 and 4 contain two clusters each. Moreover there are obvious connections between the clusters in the inverse image of intervals  $i$  and  $i + 1$  for  $i \in 1, 2, 3, 4$ . They give rise to edges in the Mapper graph presented on the right. Note that the (non-unique) enumeration of vertices comes from the enumeration of elements of the cover  $\mathcal{C}$ .

$A$  is denoted by  $v(A)$ . An undirected graph  $G$  is constructed using the following rule: for any two vertices  $v(A)$  and  $v(B)$  corresponding to clusters  $A \in C_I$  and  $B \in C_J$ , an undirected edge is placed between  $v(A)$  and  $v(B)$  if and only if  $A \cap B \neq \emptyset$ . The resulting graph  $G = (V, E)$  is called a *Mapper graph*. An illustration of the Mapper construction on a simple 2-dimensional input is shown in Figure 1.

While Mapper is a well established tool for data analysis its stability with respect to perturbation of input parameters is still open for explorations. Main results in this direction focus on convergence of Mapper graphs to the Reeb graph [36] of the manifold from which the points are sampled from, when the number of sampled points goes to infinity [4, 6]. However, the practical scope of those results is limited, especially when dealing with finite noisy samples.

Mapper and Ball Mapper are data visualization tools that provide the initial understanding of the data. Due to the stability issues, the Mapper and Ball Mapper graphs should be computed for a range of parameters and permutation of the input data, for example see Figure 7 and 8 and compared using MappingMappers or Mapper on Ball Mapper construction. The validity of any findings should be confirmed using other methods.

**2.2. Ball Mapper.** The *Ball Mapper Algorithm* introduced in [33] [34], provides a conceptually different and simpler way to obtain a cover of the input cloud  $X$  than the original Mapper. Starting from a point cloud  $X$ , and a constant  $\epsilon > 0$ , a subset  $L \subset X$  is selected having the property that for every  $x \in X$ , there exists  $l \in L$  such that  $d(x, l) \leq \epsilon$ . Such a subset  $L$  is called an  $\epsilon$ -net of  $X$

and its points are referred to as "landmarks". Algorithm 1 is an example of a greedy algorithm to compute an  $\epsilon$ -net. Other algorithms can also be used to compute  $\epsilon$ -nets [30].

**Data:** Point cloud  $X$ ,  $\epsilon > 0$

**Result:**  $L \subset X$ , an  $\epsilon$ -net

$L = \emptyset$  ;

**while** *There exists a point  $x \in X$  farther than  $\epsilon$  from every point in  $L$*  **do**

  |  $L = L \cup x$  ;

**end**

**return**  $L$

**Algorithm 1:** Greedy  $\epsilon$ -net [33].

Note that  $X \subset \bigcup_{l \in L} B(l, \epsilon)$ . The *Ball Mapper graph* is obtained by assigning each ball  $B(l, \epsilon)$  to a vertex  $v(l)$  of the graph, and by placing an edge between any two vertices whose corresponding balls jointly cover points from  $X$ . An illustration of the Ball Mapper algorithm, for the dataset from Figure 1, is shown in Figure 2.

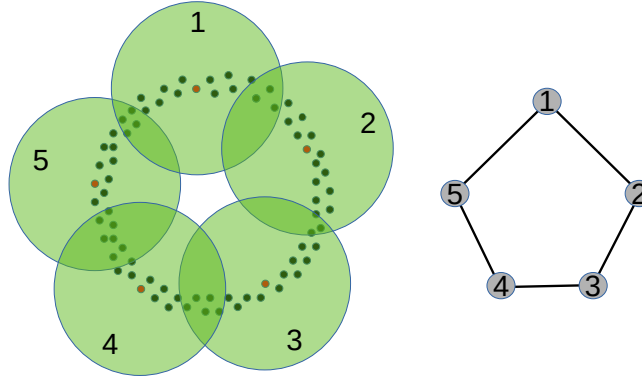


FIGURE 2. Ball Mapper construction illustration. Using the point cloud  $X$  in the Figure 1 we first select an  $\epsilon$ -net (red points in the left figure). Construct balls of radius  $\epsilon$  centered in all the points of the net (green). The union of those balls provides a cover of our data space. Ball Mapper gives a one dimensional nerve of the obtained cover. In more detail, to each ball  $B(A, \epsilon)$  we assign a vertex  $v(A)$  in the abstract graph  $G = (V, E)$ . Two balls  $B(N, \epsilon)$  and  $B(K, \epsilon)$  that jointly cover some points from  $X$  give rise to an edge between  $v(N)$  and  $v(K)$ . The Ball Mapper graph of this cover is shown on the right with the corresponding balls and vertices labeled with the same number.

**2.3. Mapper and Ball Mapper: plotting scalar-valued functions.** Let  $G$  be a Mapper or Ball Mapper graph. Its vertices cover collections of points of the input point cloud  $X$ . Therefore, given a function  $g : X \rightarrow \mathbb{R}$  we define an *induced function*  $\hat{g} : G \rightarrow \mathbb{R}$ , on  $G$ . The value of the induced function  $\hat{g}$  on a vertex  $v(A) \in G$  covering  $A \subset X$  is an average value of  $g$  over all points in  $A$ :  $\hat{g}(v(A)) = \frac{\sum_{x \in A} g(x)}{|A|}$ . Since the structure of Mapper or Ball Mapper graph  $G$  reflects the shape of the input data, visualizing the induced function on  $G$  using a color scale provides an insight into the variation of a scalar-valued function  $g$  on  $X$ . This procedure can be seen as a generalization to high dimensional samples of standards techniques, such as heatmaps, which allow for visualization

of a scalar function on a compact subset of  $\mathbb{R}^2$  by means of a color scale. To confirm that the induced function  $\hat{g}$  is a good approximation of the original function  $g$  one can consider the *variation of the values of  $g$*  on each element of the cover and compare it to the value of the induced function. If the variation is small relative to the function value  $\hat{g}$  can be used for further data analysis both in case of Mapper and Ball Mapper.

### 3. NEW DEVELOPMENTS OF MAPPER ALGORITHMS

**3.1. Equivariant Ball Mapper.** Suppose our data belongs to a metric space  $(X, d)$  with a finite automorphism group of isometries  $H$  acting on it. Although it is not necessary for the construction, in this paper we assume that the data is not noisy. Moreover, we assume that for every sample point  $x \in X$ , the data contains all elements that are in its orbit, i.e. for every  $g \in H$ ,  $g(x) \in X$ . If that is not the case, the data should be properly augmented to ensure that the sample has all the symmetries imposed by the group action. For example, see the integer-valued knot polynomials considered in Section 4.2 and the Tic-Tac-Toe endgame configurations data in Section 5.1. In case that noise is present or that data sample might not accurately reflect expected isometries, one can include the orbit of each sampled point or points in the cloud closest to the points in orbits.

Since  $H$  is an automorphism group, for every  $x, y \in X$  and every  $g \in H$ ,  $d(x, y) = d(g(x), g(y))$ . For every point  $x \in X$ , and isometry  $g \in H$  the *orbit*  $\Omega_g(x)$  of  $x$  contains the sequence of points  $x, g(x), g^2(x), \dots, g^n(x) \in X$ , where  $g^{n+1}(x) = x$  for some  $n \in \mathbb{N}$ . The relation (1) for Jones polynomial data provides a dataset with a simple automorphism group generated by a permutation of the coordinates given by the exchange matrix.

Given a point cloud  $X$  and an automorphism group  $H$  acting on it, we modify the Ball Mapper algorithm in such a way that there is an induced action of  $H$  in the Ball Mapper graph  $G$ . The induced action is described in the following way: given a vertex  $v(l) \in G$  consider  $B(l, \epsilon) \cap X$ , i.e. all the points in  $X$  covered by a ball corresponding to  $v(l) \in G$ . For every isometry  $g \in H$  we require the "covering" condition:

- all the points in  $g(B(l, \epsilon) \cap X)$  are covered by a ball  $B(g(l), \epsilon)$  and
- there are no other points in this ball.

The vertex in  $G$  corresponding to the ball  $B(g(l), \epsilon)$  is therefore denoted by  $\hat{g}(v(l))$ . Note that such  $\hat{g}$ , induced by  $g$ , is acting on an abstract graph, and therefore certain properties of  $g$  will not be reflected in  $\hat{g}$ . An example of this construction is given in Figure 3.

To ensure the "covering" condition described above is satisfied, the procedure of selection of  $\epsilon$ -net  $L \subset X$  is adjusted. In the Ball Mapper implementations  $L$  is chosen in the greedy way presented in Algorithm 1. The main idea is to add the whole orbit  $\Omega(x) = \{g(x)\}_{g \in H}$  to the constructed set of landmark points together with the any added point  $x$ . This idea is formalized in the Algorithm 2, which adjusts Algorithm 1 so that the obtained  $\epsilon$ -net  $L$  is invariant under the action of  $H$ .

**Data:** Point cloud  $X$ ,  $\epsilon > 0$ , group  $H$  acting on  $X$

**Result:**  $L \subset X$ , a  $H$ -equivariant  $\epsilon$ -net

$L = \emptyset$

**while** *There exists a point  $x \in X$  farther than  $\epsilon$  from any point in  $L$*  **do**

  |  $L = L \cup \Omega(x)$  ;

**end**

**return**  $L$

**Algorithm 2:** Equivariant greedy  $\epsilon$ -net.

Since each  $g \in H$  is an isometry, for every  $l \in L$ , if  $y \in B(l, \epsilon) \cap X$ ,  $g(y) \in B(g(l), \epsilon) \cap X$ . As each  $B(l, \epsilon) \cap X$  corresponds to a vertex in the Ball Mapper graph, the action of  $H$  on  $X$  is induced to the vertices of the Ball Mapper graph as described above.

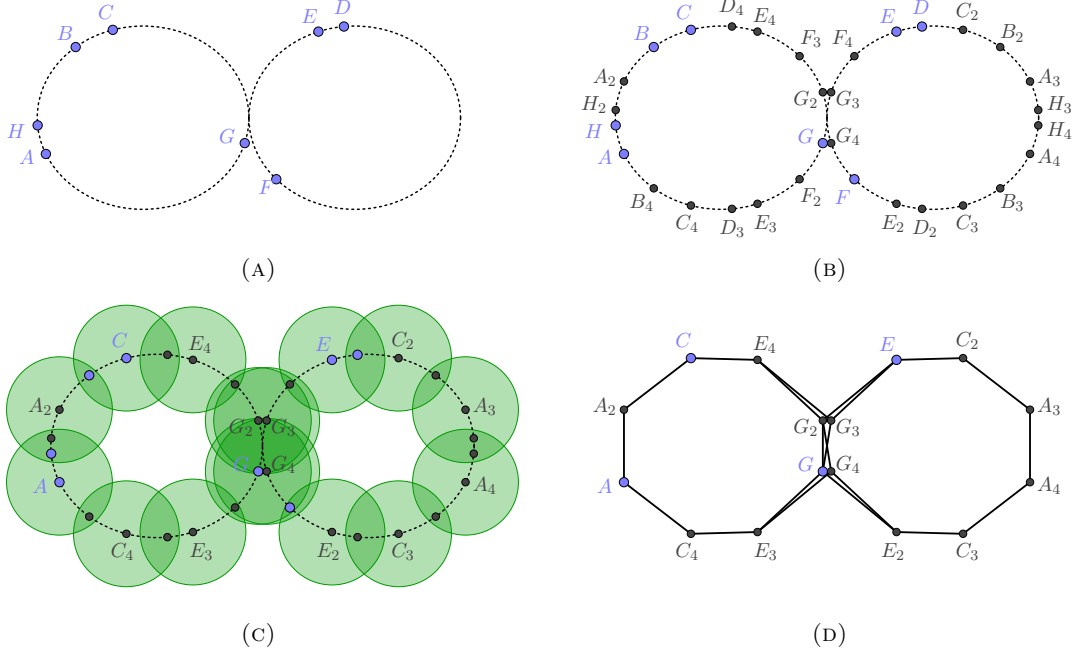


FIGURE 3. Example of the Equivariant Ball Mapper construction on a point cloud  $X$  sampled from a wedge of two circles (A) with a symmetry group determined by the reflections on the horizontal and vertical axis. The point cloud enriched by each point's orbit is shown in (B). Selected landmarks  $A, C, E$  and  $G$ , and all the points in their orbits that are selected as well are shown in (C) with a covering consisting of 16 balls. The resulting equivariant Ball Mapper graph is depicted in (D).

In Algorithm 2, the *while* loop iterates once through the points in  $X$ . The time needed to locate all points at a distance less or equal than  $\epsilon$  to a given point is bounded by  $|X|$ , hence the overall complexity of the presented procedure is bounded by  $|X|^2$ .

This equivariant construction is Ball Mapper specific and it is not clear that the analogous construction for Mapper is possible. For example, the equivariant Mapper construction requires the lens function to be either invariant with respect to the group action (i.e. points in the same orbit should obtain the same value of the function), or to map points from the input point cloud to different cover elements in such a way that there is an induced group acting on the cover. Adjusting the lens function to satisfy either of this requirements is non-trivial and also requires the clustering algorithm to be performed in such a way that there is an appropriate group action induced on the obtained clusters. These obstacles to obtaining equivariant Mapper emphasize the advantage of Ball Mapper with respect to equivariance and justify our choice.

**3.2. Mapper on Ball Mapper.** This section provides a new construction of a Mapper graph, as described in Section 2.1. It uses the output of the Ball Mapper algorithm, described in Section 2.2 to cover the range of the lens function.

Recall that the Mapper construction is based on a interval cover of the range of the lens function  $f : X \rightarrow \mathbb{R}^n$ . Typically  $n = 1$  or another small positive integer, as the range of  $f$  needs to be covered with a collection of overlapping cubes, defined as a product of intervals. There is antagonism between wanting large  $n$  when the lens function is more likely to preserve essential information about the point cloud, and the fact that having  $k$  intervals in each of  $n$  directions requires  $k^n$  cover elements which is not computationally feasible for large values of  $n$ .

To overcome this obstacle we propose the following *Mapper on Ball Mapper (MoBM)* construction to leverage the overlapping, adaptive cover of the point cloud obtained from Ball Mapper. This algorithm applies to the more general setting with two point clouds  $X, Y$  and a relation  $p : X \rightarrow Y$ . MoBM is formalized by the following pseudocode:

**Data:** Point clouds  $X, Y$ , a relation  $p : X \rightarrow Y$ ,  $\epsilon > 0$ , a clustering algorithm  $C$

**Result:** MoBM graph representing  $X$

Let  $\{B(l, \epsilon)\}_{l \in L}$  be the balls in a Ball Mapper of  $p(X)$  constructed for the radius  $\epsilon$ ;

Apply  $C$  to each  $\{p^{-1}(B(l, \epsilon)) \cap X\}_{l \in L}$  to obtain an overlapping cover of  $X$ ;

MoBM = 1-dimensional nerve of such cover;

**return** MoBM

**Algorithm 3:** Mapper on Ball Mapper.

This construction, illustrated in Figure 4, requires only two parameters: the radius  $\epsilon$  and the choice of the clustering algorithm. There is no need to define the number of intervals or the overlapping percentage as in the conventional Mapper algorithm; the covering of  $Y$ , being the range of the lens, is completely determined by the Ball Mapper graph. However, varying the selection of landmark points can lead to potentially different Ball Mapper graphs. Selection of different landmarks can be obtained by permuting the points of  $Y$  and re-running the algorithm. The time complexity of MoBM is bounded by the time required to run both Mapper and Ball Mapper.

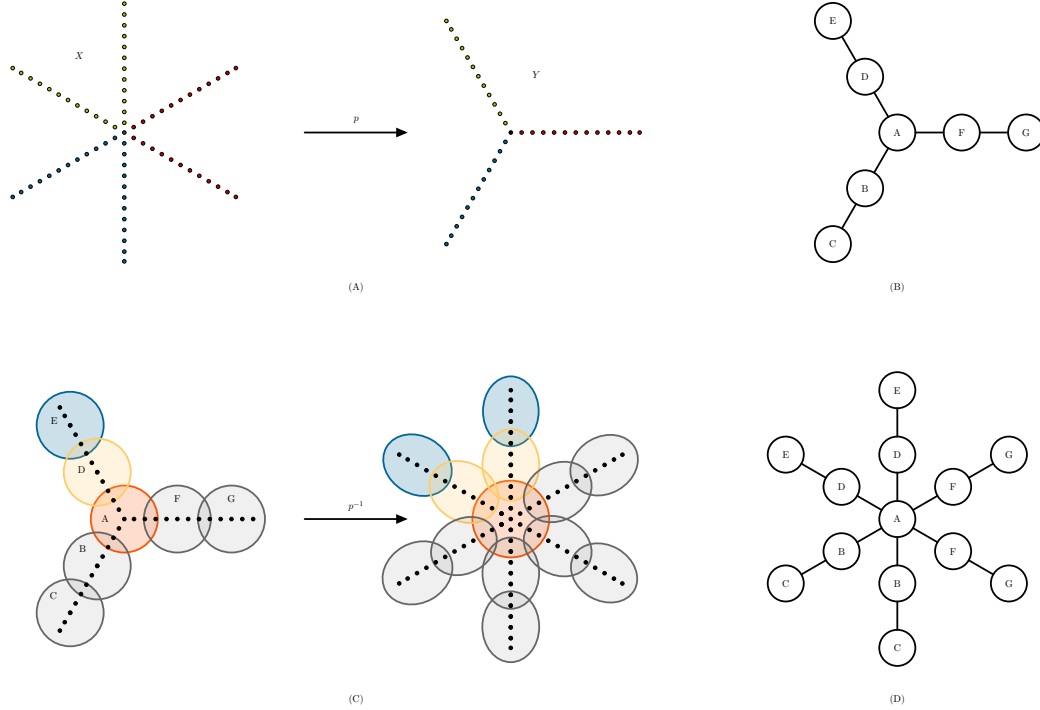


FIGURE 4. The Mapper on Ball Mapper construction: an illustration. The point cloud  $X$  is mapped via  $p$  to the point cloud  $Y$  (A) where the map is indicated by corresponding colors. The Ball Mapper graph for  $Y$  (B) is used to obtain a cover of  $Y$  (C, left). Such cover is then pulled-back to obtain a covering of  $X$  (C, right). The resulting Mapper on Ball Mapper graph for  $X$  is shown in (D), where, similarly to Figure 1, node labels indicate the originating covering ball in  $Y$ .

**3.3. MappingMappers.** The standard construction of Mapper or Ball Mapper for a point cloud  $X$  with a metric  $d : X \times X \rightarrow \mathbb{R}^{\geq 0}$  provides a model of the point cloud  $X$ . If the point cloud  $X$  is equipped with a function  $f : X \rightarrow \mathbb{R}$ , an induced function  $\hat{f}$  can be defined on the Mapper or Ball Mapper graph  $G$  as explained in Sections 2.1 and 2.2. This way, Mapper and Ball Mapper graphs can be used to visualize functions  $f : \mathbb{R}^n \rightarrow \mathbb{R}$ , where  $f$  is defined on  $X \subset \mathbb{R}^n$ .

Consider a more general question of using Mapper and Ball Mapper to visualize functions  $f : \mathbb{R}^n \rightarrow \mathbb{R}^m$  for larger values of  $m$  and  $n$ . Assume that we are given  $X \subset \mathbb{R}^n$  and  $Y \subset \mathbb{R}^m$  and a relation  $f \subset X \times Y$  (note that a function is a particular case of such a relation). In this instance we focus on the Ball Mapper-based construction. A construction for Mapper is analogous. In the first step, let us build Ball Mapper graphs  $G(X)$  and  $G(Y)$  corresponding to point clouds  $X$  and  $Y$  and denote with  $V(X)$  and  $V(Y)$  the corresponding vertex sets. Given a relation  $f \subset X \times Y$  assigning points from  $X$  to the points from  $Y$ , define a map  $\tilde{f} : V(X) \rightarrow [0, 1]^{V(Y)}$  in the following way. For every  $v$  in  $V(X)$ , corresponding to a ball  $B(l_X, \epsilon_X)$  compute  $f(B(l_X, \epsilon_X) \cap X) \subset Y$ . For every vertex  $w$  in  $V(Y)$  corresponding to a ball  $B(l_Y, \epsilon_Y)$ , compute  $\frac{|B(l_Y, \epsilon_Y) \cap f(B(l_X, \epsilon_X) \cap X)|}{|B(l_Y, \epsilon_Y) \cap Y|}$ . This fraction indicates the percentage of points in  $B(l_Y, \epsilon_Y) \cap Y$  that are in the image of the points covered by the vertex  $v$  in  $G(X)$ . When computed for every vertex in  $G(X)$ , this fraction gives us  $|V(X)|$  different coloring functions on  $G(Y)$  indicating where the image of each vertex  $v$  is mapped.

This construction works analogously for arbitrarily large unions of vertices of the graph  $G(X)$ . The procedure described above is automatized and a reliable interface can be found in [10]. It allows to see which regions of  $G(Y)$  corresponds to chosen region of  $G(X)$ . By doing so, a visualization of the map  $f : X \rightarrow Y$  is obtained. A simplified example of the procedure is given at the Figure 5.

#### 4. APPLICATIONS: KNOT THEORY

Analyzing and visualizing data from knot theory is the main motivation and inspiration for the development of algorithms presented in Sections 3.1, 3.3 and 3.2. This section discusses the basis of knot theory and the data used in the our analysis, followed by the results obtained using Equivariant Ball Mapper, Mapper on Ball Mapper, and MappingMappers.

**4.1. Knot theory: a brief introduction.** A knot is a class of embeddings of  $S^1$  into  $\mathbb{R}^3$  up to ambient isotopy [25, 24, 18]. Knots are hard to distinguish and their classification and tabulation [16, 15, 2, 26, 5] solicits techniques from a range of mathematical disciplines. Consequently, a number of *knot invariants* have been introduced in an attempt to compare and classify knots. A knot invariant should be thought of as a quantity assigned to each knot such that if two knots are the same (isotopic), the values assigned to them are the same. The most common knot invariants are integers, one- or two-variable polynomials, groups, etc. In this paper we focus on the following knot invariants and their relations:

- Numerical: minimal crossing number, signature  $\sigma(K)$  [21] defined as a signature of a matrix obtained using a Seifert surface.
- Polynomial: Alexander  $\Delta(K)(t)$  [1], Jones  $J(K)(q)$  [20],  $P(K)(a, z)$  HOMFLYPT [13].

Since knot invariants often rely on advanced algebraic, geometric, and combinatorial topology, in lieu of definitions we provide references [25, 37, 24, 18], and key insights sufficient for analyzing these knot invariants and their relations. Note that Alexander and Jones polynomials are 1-variable polynomials, while HOMFLYPT polynomial is of two variables. Moreover, HOMFLYPT is more general than both the Alexander and Jones polynomial. HOMFLYPT specializes to the Jones polynomial [20] by substituting  $a = t^{-1}$  and  $z = \sqrt{t} - \frac{1}{\sqrt{t}}$ , and to the Alexander polynomial [1] by substituting  $a = 1$  and  $z = \sqrt{t} - \frac{1}{\sqrt{t}}$ .

Note that it is common for knot tables to contain only one knot from each mirror pair  $(K, \text{mir}(K))$ , since if a knot  $K$  is achiral it coincides with its mirror  $\text{mir}(K)$ , and many invariants either do not



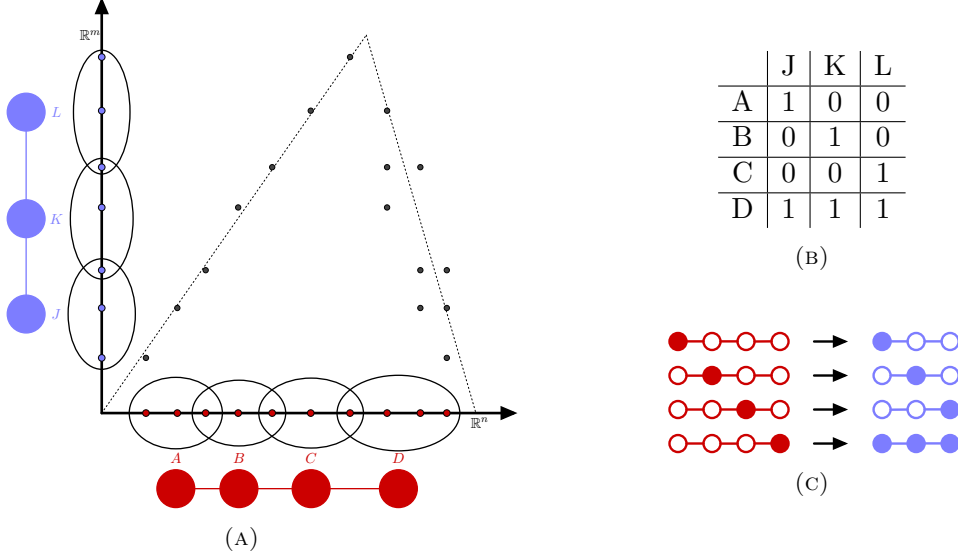


FIGURE 5. Consider a relation  $f$  between  $X \subset \mathbb{R}^n$  located on the x-axis and  $Y \subset \mathbb{R}^m$  on the y-axis, represented by the black dots in the plane, see (A). Next, create Ball Mapper graphs on both domain  $X$  and co-domain  $Y$ . Set  $X$  is covered by four balls corresponding to the red vertices in the Ball Mapper graph, while  $Y$ , with the three balls corresponding to the blue vertices in the Ball Mapper graph. Based on the relation, the points in  $X$  covered by  $A$  are mapped into points covered by  $J$  in  $Y$ . Similarly,  $B$  into  $K$ ,  $C$  into  $L$ . Lastly, the points in  $D$  in  $X$  are mapped to points in  $J$ ,  $K$  and  $L$ . In addition, when we track the proportions of points in each of the ball  $J$ ,  $K$  and  $L$  that are reached by points in  $A$ ,  $B$ ,  $C$  or  $D$ . Such proportions are indicated in the matrix (B). Each row in this matrix provides a coloring function on the image Ball Mapper graph (C). This idea generalizes and provides a way to visualize maps between point clouds in high dimensional spaces.

| Invariant | Unknot | Trefoil                | Data vector                            |
|-----------|--------|------------------------|--|
| Alexander | 1      | $t^{-1} - 1 + t$       | (0,1,-1,1,0)                           |
| Jones     | 1      | $q + q^3 - q^4$        | (0,0,0,0,0,1,0,1,-1)                   |
| HOMFLYPT  | 1      | $-a^4 + 2a^2 + a^2z^2$ | (0,0,0,0,0,0,2,0,-1,0,0,0,0,0,0,1,0,0) |

TABLE 1. Values of several knot polynomials for the unknot and the trefoil, and the corresponding data vector. Note that for the 2-variable HOMFLYPT polynomial the coefficient matrix is flattened into a vector: the variable  $z$  corresponding to rows,  $a$  to columns.

distinguish between mirrors or have a straightforward relation between the two values. The Alexander polynomial does not distinguish between the knot and its mirror, and the Jones polynomial [24, 20] satisfies the following relation:

$$(1) \quad J(\text{mir}(K))(q) = J(K)(q^{-1}).$$

The signature of a knot and its mirror have opposite signs [24],

$$(2) \quad \sigma(\text{mir}(K)) = -\sigma(K).$$

and for the HOMFLYPT polynomials of mirror knots the following relation holds:

$$(3) \quad P(\text{mir}(K))(a, z) = P(K)(a^{-1}, z)$$

**4.2. Knot invariants as point clouds.** The use of big data techniques [17, 19, 40, 22] is warranted by the result of Ernst and Summers showing that the number of knots with a given number of crossings grows exponentially [11]. The point clouds are obtained in the way introduced and described in [22], where each knot is represented by a vector of coefficients of a knot polynomial such as the Alexander, Jones or HOMFLYPT polynomial. The datasets we consider were created by J.S. Levitt [22], and preprocessed by D. Gurnari. The data is freely available at [10] and includes Alexander and Jones polynomials, together with numerical knot invariants like minimal crossing number and signature for all 9755329 knots up to 17 crossings. HOMFLYPT polynomials are provided for all 313231 knots up to 15 crossings.

Following [22], given a finite collection of knots  $\mathcal{K}$ , we construct a point cloud  $\mathcal{I}(\mathcal{K})$  corresponding to the coefficients of the one-variable polynomial invariant  $\mathcal{I}$ , in the following way:

- Step 1 Given a knot  $K \in \mathcal{K}$  and its single variable polynomial  $I(K)$ , extract a vector of the coefficients.
- Step 2 Compute the minimal and maximal powers  $\min_t, \max_t$  of the variable denoted by  $t$  among all knots in  $\mathcal{K}$ . Then the maximal length of all considered vectors is  $d = \max_t - \min_t + 1$ .
- Step 3 Add zeros on both sides of each vector of coefficients to obtain a vector  $I(K)_v \in \mathbb{R}^d$  to ensure a correct alignment of corresponding powers.

Note that in this way all vectors are of the same length determined by the overall minimum and maximum exponent, and, the coefficients of a given power are in the same position in the vector for all the considered knots. In case of a two-variable polynomial, such as the HOMFLYPT polynomial, we apply Steps 1-3, as described above in the case of one-variable polynomial, to both variables. In this way we first obtain a matrix padded with zeros, and then create a corresponding vector by linearizing this matrix (concatenating its rows). HOMFLYPT data belongs to  $\mathbb{R}^d$  where  $d = (\max_a - \min_a + 1)(\max_z - \min_z + 1)$  where  $a$  and  $z$  stand for the two variables in the corresponding polynomial. Examples of the coefficient vectors obtained from both the unknot and the trefoil are presented in Table 1.

Unlike some databases, we choose to consider knots and their mirrors although that increases the dimension of the point cloud coefficient vectors. The Jones coefficient vector of its mirror is obtained by reversing the original vector, see (1), and therefore the point cloud admits a symmetry given by the exchange matrix. The HOMFLYPT coefficient matrix of the mirror knot can be obtained by reversing the columns of the original matrix (3). Hence, in the case of the Jones polynomial  $\min_t(\text{mir}(K)) = -\max_t(K)$  and  $\max_t(\text{mir}(K)) = -\min_t(K)$  as a consequence of relation (1) and the point cloud belongs to  $\mathbb{R}^d$  where  $d = 2\max(|\max_t|, |\min_t|) + 1$ .

The size of the obtained tables of polynomial coefficients are the following: 9755329 rows  $\times$  17 columns for Alexander, 19510658 rows  $\times$  51 columns for Jones and 626462 rows  $\times$  152 columns for HOMFLYPT. Note that the number of rows in Jones and HOMFLYPT data is double the number of prime knots since mirrors are also included.

**4.3. Ball Mapper: structure of knot polynomial data.** In this section we apply standard and Equivariant Ball Mapper to data obtained from Jones, Alexander and HOMFLYPT polynomials for all knots up to 17 crossings. The choice to use Ball Mapper is natural, as there is no obvious lens function for the Mapper construction.

Since our data contains knots and their mirror images, the Jones polynomial data cloud admits a symmetry generated by the permutation of the coordinates for those knots which are not identical to their mirrors (see (1)). Figure 6 shows Ball Mapper graphs with just one of the mirrors included (A), knots and their mirrors with the standard Ball Mapper (B) and the equivariant Ball Mapper

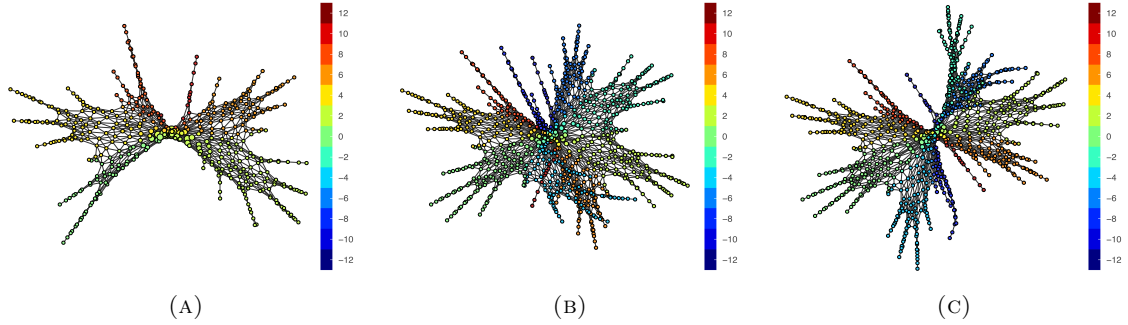


FIGURE 6. Ball Mapper applied to Jones polynomial data of knots up to 17 crossings with just one choice of a mirror (A), knots and their mirrors with standard Ball Mapper (B) and Equivariant Ball Mapper (C). Color reflects the average signature of knots in each cluster. Note that the graph in (C) is symmetric, although this fact is not accurately represented in this image due to the chosen graph plotting subroutine.

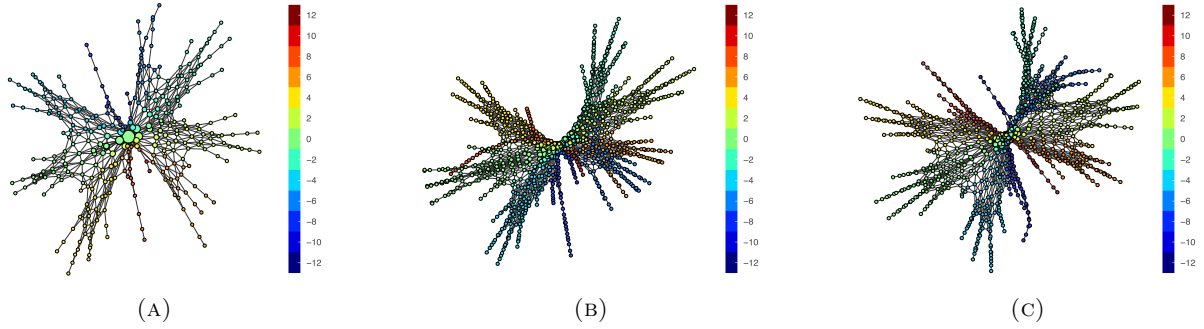


FIGURE 7. Stability of Equivariant Ball Mapper for Jones polynomial data with respect to the crossing number filtration: EqBM graphs of knots up to 15 crossings  $\epsilon = 30$  with 826 nodes (A), 16 with  $\epsilon = 50$  with 1008 nodes (B), 17 crossings with  $\epsilon = 100$  with 890 nodes (C).

construction from Section 3.1 in 6(C). The symmetry of the data is preserved by the equivariant Ball Mapper (C): for each flare there is an identical one with opposite signature, as a consequence of relation (2).

The structure of the BM graph is stable with respect to the filtration by the number of crossings, as illustrated in Figure 7, in addition to stability across the choice of parameter/radius shown as shown in Figure 8. This observation is important since sampling knot data is a hard problem and it is known that knots with lower crossing number do not provide a sample representative of the space of knots [22].

The Ball Mapper graph for the Alexander polynomial data has linear structure, see Figure 9(B). The two flares contain clusters of knots whose signature modulo 4 is equal to zero or two, respectively. Similarly, the Ball Mapper graphs for HOMFLYPT data exhibit a star-like structure whose flares contain knots with the same signature, Figure 9(C). As in the case of the Jones polynomial data, all Ball Mapper graphs are stable with respect to the crossing number filtration and the choice of Ball Mapper parameter  $\epsilon$ .

**4.4. MappingMappers and Mapper on Ball Mapper: comparing knot invariants.** In this section, we further investigate data corresponding to the Jones, Alexander, and HOMFLYPT

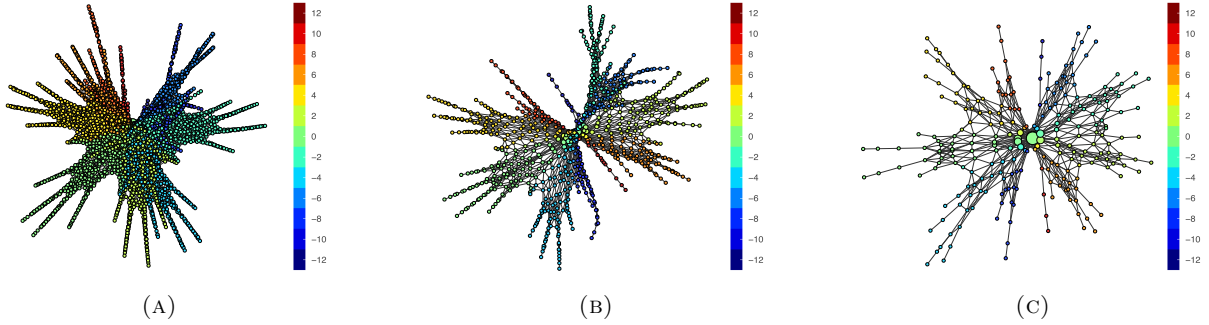


FIGURE 8. Stability of Equivariant Ball Mapper with respect to the choice of parameter/radius  $\epsilon$ : EqBM graphs of knots up to 17 crossings  $\epsilon = 50$  with 3840 nodes (A),  $\epsilon = 100$  with 890 nodes (B),  $\epsilon = 200$  with 254 nodes (C). Color is determined by the average signature of knots in that node/cluster.

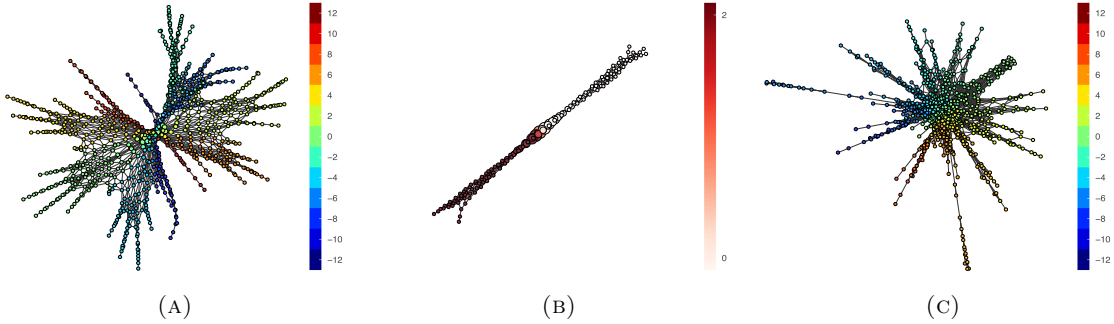


FIGURE 9. Equivariant Ball Mapper graphs for the Jones (A), Alexander (B), and HOMFLYPT (C) polynomial data of knots up to 17 crossings colored by the average signature of knots in each cluster (A), (C) or signature mod 4 in (B).

polynomials whose Ball Mapper graphs are provided in Section 4.3. The main goal is to compare these spaces using Ball Mapper based tools developed in Sections 3.3 and 3.2, in order to, implicitly, compare the invariants. First, spaces of two invariants can be compared by constructing their Ball Mapper graphs and visualizing the maps between them as described in Section 3.3. Next, Mapper on Ball Mapper construction from Section 3.2 is used to emphasize relative strengths of two invariants with respect to distinguishing knots. To be more specific, given two invariants  $A$  and  $B$ , in general data descriptors, of a dataset  $\mathcal{K}$  we can think of them as maps  $A : \mathcal{K} \rightarrow M_A$  and  $B : \mathcal{K} \rightarrow M_B$ , where  $M_A$  and  $M_B$  are metric spaces. Most commonly,  $M_A$  and  $M_B$  are finite point clouds in Euclidean spaces of different dimensions. Inspired by comparison of knot invariants, that invariant  $A$  is considered to be *stronger* than invariant  $B$  if the elements covered by a single vertex or several closely-connected vertices in the Mapper on Ball Mapper graph of  $M_B$  are spread across different regions of the Mapper on Ball Mapper graph of  $M_A$ . MappingMappers and Mapper on Ball Mapper can be used for this type of analysis.

MappingMappers, defined in Section 3.3, uses two point clouds  $X \subset \mathbb{R}^n$  and  $Y \subset \mathbb{R}^m$  and a relation  $f \subset X \times Y$  as inputs. To illustrate this technique we use the collection  $\mathcal{K}$  of knots up to 17 crossings along with the Jones  $J(\mathcal{K}) \subset \mathbb{R}^{51}$  and the Alexander  $A(\mathcal{K}) \subset \mathbb{R}^{17}$  point clouds obtained in Section 4.2.

Using the set of knots  $\mathcal{K}$  as the common indexing set, we define the relation  $f \subset A(\mathcal{K}) \times J(\mathcal{K})$  in the following way: for a given knot  $K \in \mathcal{K}$  its Alexander polynomial  $A(K)$  in  $A(\mathcal{K})$  is related

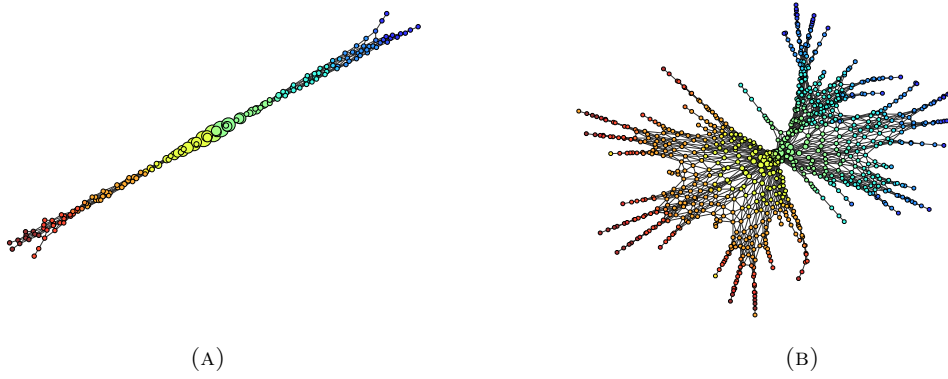


FIGURE 10. MappingMappers: Representation of a map from the space of the Alexander (A) and the space of the Jones polynomials of knots up to 17 crossings (B). Rainbow coloring of consecutive clusters of the linear embedding of the Equivariant Ball Mapper graph for the Alexander data and used to color the corresponding regions of the Equivariant Ball Mapper graph for the Jones data.

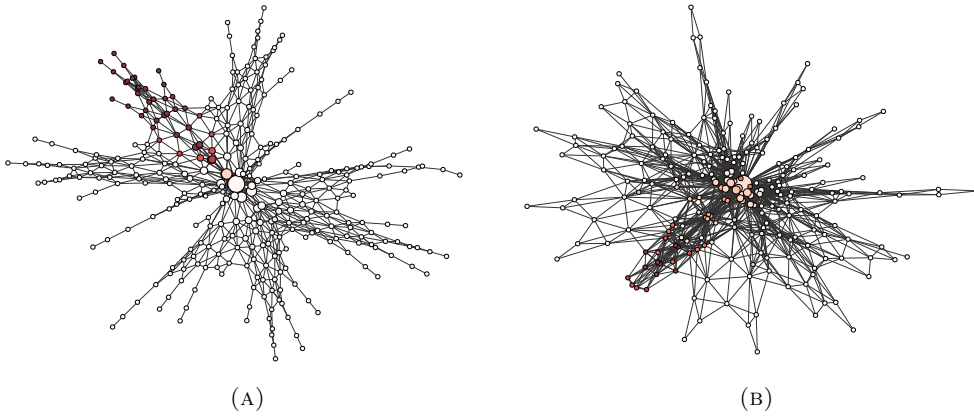


FIGURE 11. MappingMappers: Visualizing the map from the space of Jones polynomials to the space of HOMFLYPT polynomials of knots up to 15 crossings using the Ball Mapper graph (containing 326 nodes) of Jones polynomial with  $\epsilon = 50$  (A) and the Ball Mapper graph (containing 258 nodes) of HOMFLYPT polynomial of with  $\epsilon = 50$  shown in (B). All clusters containing knots with signature equal to zero in both Ball Mapper graphs are shown as a shade of red.

to its Jones polynomial  $J(K)$  in  $J(\mathcal{K})$ . Note that this is a relation rather than a function, since some knots from  $\mathcal{K}$  may have the same Alexander polynomial, but different Jones polynomials, and vice versa. In this case, a single point from  $A(\mathcal{K})$  can be related to multiple points of  $J(\mathcal{K})$  or the other way around. Figure 10 illustrates this relation: colors indicate matching regions in the Alexander and Jones Ball Mapper graphs. Roughly speaking, the linear structure of the Alexander Ball Mapper induces the linear structure among the flares in the star-like Ball Mapper graph of the Jones data. In the opposite direction, flares of the Jones Ball Mapper merge according to the signature module 4 which is consistent with the fact that one end of the Alexander Ball Mapper contains knots whose signature mod 4 is zero and the other one is two. Figure 11 illustrates the analogous relation between the Jones and HOMFLYPT Ball Mapper graphs, respectively. The

non-linear nature of the Jones Ball Mapper graph prohibits using a gradient-like coloring; instead, the cluster color in this graph reflects the percentage of knots with signature equal to zero and the corresponding clusters in the HOMFLYPT Ball Mapper graph.

To illustrate how methods introduced in this paper can be used to discover potentially new results in knot theory, let us reconsider the Ball Mapper graph in Figure 9(B). The distribution of signature values suggests that signature mod 4 can be determined as a function of the coefficients of the Alexander polynomial. This hypothesis was tested by training a Support Vector Machine classifier [3]. According to it, the perfect separation between two classes of knots, those whose signature mod 4 is zero and those with it equal to 2, is achieved with an "anti-diagonal" hyperplane with normal vector  $[1, -1, 1, \dots]$ . This observation indicates that the sign of the alternating sum of the coefficients of the Alexander polynomial determines the signature mod 4. The correspondence between clusters of Ball Mapper graphs of the Alexander and Jones polynomials shown in Figure 10 suggests that analogous property should hold for the Jones polynomial. Turns out that both statements are true according to the well-known theorem [7]. Our approach provides a new way of obtaining such theorem and paves the way for using mapper-type algorithms to aid discovery in knot theory in particular and theoretical mathematics and sciences in general.

Next, we employ MoBM on the algebraic relation between the HOMFLYPT polynomial and both the Alexander and Jones polynomials, see Section 4.1. These specializations tie in with the framework introduced in Section 3.2 as they can be used as lenses for Mapper algorithm when using the Mapper on Ball Mapper, or MoBM, construction.

As a clustering method in the MoBM construction, we use the DBSCAN algorithm [12]. DBSCAN requires a new parameter  $\epsilon_{DB}$  in addition to the  $\epsilon$  denoting the radius of balls used in the Ball Mapper construction.

The MoBM construction using knots data is illustrated in Figure 12: Ball Mapper on Jones data Figure 12 (A) is used as the input covering to the MoBM graph 12 (B) the HOMFLYPT data whose Ball Mapper is in Figure 11(B). The coloring in Figure 12 (A) represents the number of clusters into which the points in each node split when they are pulled back from the space of Jones to HOMFLYPT. This pullback is not trivial (clusters split into more than one cluster in the pre-image) in the center region and in between the flares. The obtained MoBM graph thus achieves better separation in those regions.

## 5. APPLICATIONS: GAME THEORY, MATERIALS SCIENCE AND CANCER RESEARCH

The techniques discussed in this paper apply to a wide range of datasets. In this section we present additional sample applications of the proposed techniques to artificial datasets, game theory, materials science and cancer research.

**5.1. Equivariant Ball Mapper: Tic-Tac-Toe data.** Any dataset with a nontrivial isometric group action can be visualized with preservation of the action using Equivariant Ball Mapper. As an example we analyze the Tic-Tac-Toe endgame dataset [9] that consists of all possible board configurations at the end of Tic-Tac-Toe games. These configurations, numbering 958 in total, are represented by 3 by 3 matrices (interpreted as vectors in  $\mathbb{R}^9$ ) since the game is played between two players on a 3 by 3 grid where the first player places noughts and the second places crosses. The winner is the first player who places three noughts or crosses in a vertical, horizontal or a diagonal line.

The input for our analysis consists of 3 by 3 grids, interpreted as vectors with 9 entries, with values  $-1$  (corresponding to a nought),  $0$  (corresponding to an empty slot) or  $1$  (corresponding to a cross). The symmetries of the  $3 \times 3$  configurations are given by a dihedral group consisting of four rotations and four reflections. It is straightforward to see that all configurations in one orbit are all wins, loses or ties, since rotation and reflection of the board does not change the outcome

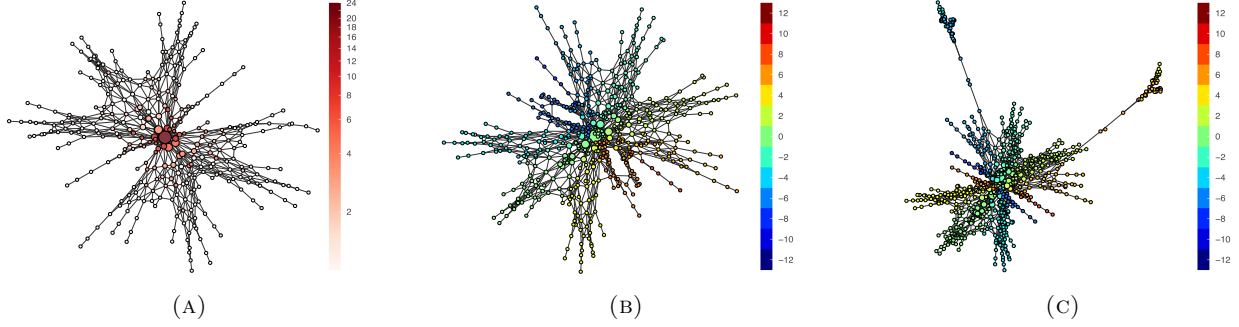


FIGURE 12. The Mapper on Ball Mapper graph on Jones-HOMFLYPT data pair. Image (A) shows the Ball Mapper graph for Jones data for knots up to 15 crossings at  $\epsilon_{BM} = 50$  with a total of 326 nodes colored by the number of clusters found in each node. The Mapper on Ball Mapper construction in (B) is obtained from the Jones Ball Mapper (A) and the HOMFLYPT data for the DBSCAN clustering algorithm parameter equal  $\epsilon_{DB} = 40$  with 644 nodes, and colored by signature. Analogous MoBM construction for  $\epsilon_{DB} = 30$  reveals a different structure on HOMFLYPT data (C): the two long flares emerging in (C) consist knots with the same s-invariant [35], but different values of signature.

of the game. These symmetries induce relations between vectors in  $\mathbb{R}^9$  and the Euclidean distance between any two configurations and their images via one of the actions will be the same. Hence, Equivariant Ball Mapper is the natural choice for this data; see the resulting Ball Mapper graph in the Figure 13(A).

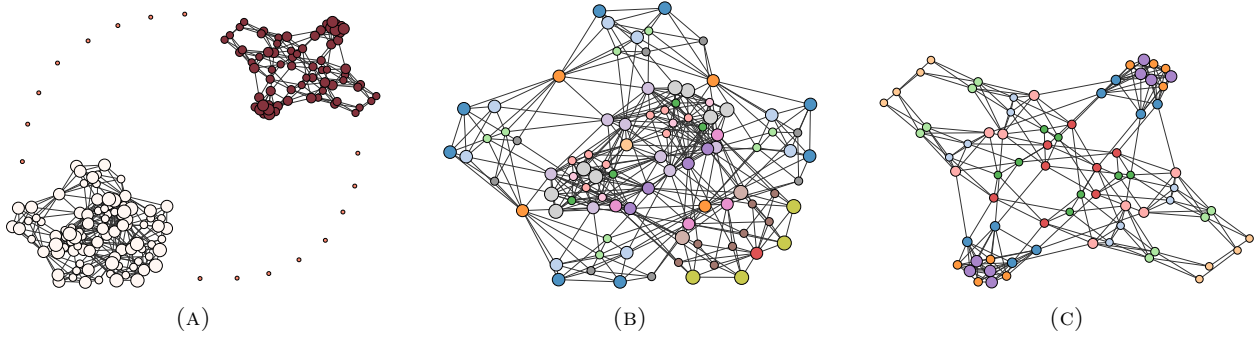


FIGURE 13. The Equivariant Ball Mapper graph for the Tic-Tac-Toe dataset. Figure 13c shows the game outcome: the wins clusters are colored white, the losses clusters red. The sixteen isolated orange clusters correspond to all possible ties. The wins and losses clusters are shown in 13b and 13c respectively, with color denoting orbits. Note that even if the same color palette is used, there is no relation between the nodes in 13b and 13c as the dihedral symmetry does not change the outcome of a game.

While our purpose is to showcase the technique rather than to draw a conclusion about the output, we include several observations. The Equivariant Ball Mapper graph for radius  $\epsilon = 2.5$  (using  $l_1$  distance) provides a perfect separation between the configurations in which the first player wins the game (white), loses the game (red) or when there is a tie (orange), see Figure 13(A). We attribute the clear separation of win-loss-tie clusters, as well as the symmetries of the win clusters



(Figure 13(B)) and loss clusters (Figure 13(C)), to the combinatorial properties of the game. In panels (B) and (C) nodes belonging to the same orbit are colored with the same color. Note that different orbits might have different lengths. A configuration with no rotation or reflection symmetry will lead to a length 8 orbit. On the other hand, a configuration that already has some symmetries will have a shorter orbit. The maximally symmetric configuration has an orbit of length 1. This corresponds to the only red node in the bottom right of Figure 13(B). Intuition on the perfect win-loss-tie separation can be built by considering the smallest  $l_1$  distance between configurations. It is not difficult to show that the distance between winning and losing configurations is at least 3. Similarly, the minimum distance between two ties is 4 and the minimum distance between winning (resp. losing) configuration and a tie is 4 (resp. 3). On the other hand, any pair of winning (resp. losing) configurations can be connected by a sequence of winning (resp. losing) configurations spaced by at most 2. In lieu of the proof, consider a Ball Mapper graph with radius  $2 < \epsilon < 3$ , like the one depicted in Figure 13(A), where all the winning (resp. losing) configurations are in the same connected component evidencing the existence of such a path.

**5.2. MappingMappers: superconductors.** As an example of a map between two set of descriptors of the same data, we consider the superconductor dataset available from the UC Irvine Machine Learning Repository [14].

The dataset contains two descriptors of a family of 21263 superconductors. The first one, the *characteristics dataset*, is composed of 81 features extracted from considered superconductors. The other, the *composition dataset*, contains sparse vectors in  $\mathbb{R}^{86}$  that describe the chemical composition of the superconductor.

A Ball Mapper graph for the characteristic dataset, with all features scaled to the interval  $[0, 1]$  and with radius  $\epsilon = 2$ , is provided in Figure 14(A). For the composition dataset, the Ball Mapper for any fixed radii is either composed of a single vertex, or a large group of small, disconnected clusters. We attribute this behavior to a concentration of measure-type phenomena. In order to construct a meaningful Ball Mapper graph, we use a cosine similarity measure [32] instead of the standard Euclidean metric. The corresponding Ball Mapper graph obtained for  $\epsilon = 0.25$  is shown in Figure 14(B). The red color in both Ball Mapper graphs on Figure 14 denotes superconductors that work in the highest temperature and should be easiest to use in practice.

Next we can compare structures of the two datasets characterizing superconductors using MappingMappers since the data is related via the map described in [14]. MappingMappers (figure not presented for brevity) shows that the image of a single vertex in the Ball Mapper graph of one of the datasets contains multiple disconnected regions in the second one. These results suggest that the characteristic and composition data provide distinct and likely unrelated information; hence, when analyzed together, these should provide more insights into properties of superconductors.

**5.3. Mapper on Ball Mapper.** Last but not least, we illustrate the performance and properties of Mapper on Ball Mapper on both synthetic and real-word datasets.

**5.3.1. Nonlinear datasets.** Our first artificial dataset is based on a set  $C$  obtained by sampling 500 points from the nonlinear embedding  $F : \mathbb{R}^2 \rightarrow \mathbb{R}^7$  defined by  $F(x, y) = (xy, x^2, y^2, x^2y, y^2x, x^3, y^3)$  of the unit circle in  $\mathbb{R}^2$ . The Ball Mapper graph of  $C$  is a cyclic graph, recovering the topology of the original unit circle. Then we take the Cartesian product of  $C \times L$  where  $L$  is a uniform sample of 100 points from the unit interval  $[0, 10]$ . This data set consists of  $500 \cdot 100 = 50000$  points in  $\mathbb{R}^8$  and its shape comes from a cylinder with a unit base circle embedded in  $\mathbb{R}^8$  via the product of  $F$  with the identity map.

The Ball Mapper graph of  $C \times L$ , shown on Figure 15a, recovers the cylindrical shape for a sufficiently small radius. However, the resulting Ball Mapper graph contains a large number of nodes and could be difficult to interpret. More importantly, if the radius is increased a bit, the



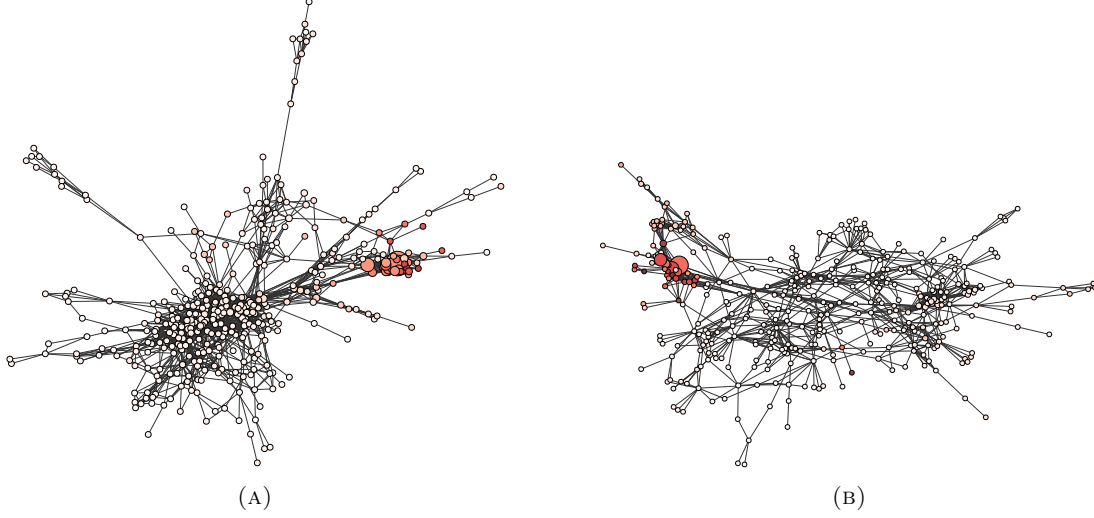


FIGURE 14. Ball Mapper graphs of the superconductor characteristic (A) and composition dataset (B) for superconductor datasets available from the UC Irvine Machine Learning Repository, colored by critical temperature.

base cycle in the Ball Mapper graph would collapse to a point and the information about the central hole would be lost.

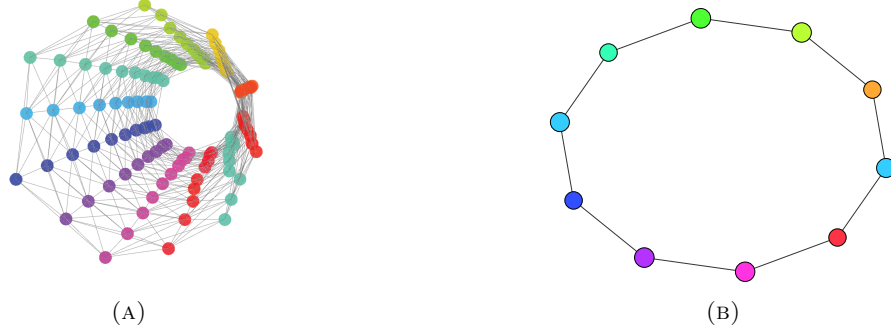


FIGURE 15. The Ball Mapper graph obtained from  $C \times L$  data is shown in (A). A sufficient small  $\epsilon$  has to be chosen in order to observe the central hole, which leads to a lot of nodes being created. On the other hand, the Mapper on Ball Mapper graph obtained by pulling back the points covered by the nodes in the Ball Mapper graph on  $C$  to  $C \times L$  is presented in (B). The coloring on both graphs is a function of the angle  $\alpha = \cos^{-1}(x)$  and it used to show the correspondence between the Ball Mapper of the space  $C$  and the MoBM for the space  $C \times L$ .

Since these two datasets are related via the projection  $\pi : C \times L \subseteq \mathbb{R}^8 \rightarrow C \subseteq \mathbb{R}^7$ , which takes each point in  $C \times L$  to its component in  $C$ , we can apply the Mapper on Ball Mapper construction on  $C$  and  $C \times L$  using the projection map  $\pi$  as a lens. The Mapper on Ball Mapper graph, shown on Figure 15(B), captures the shape of the base space  $C$  which is a cycle. Moreover, each copy of  $L$  in  $C \times L$  contains only one cluster, hence can be considered to be a single connected component. The Mapper on Ball Mapper graph, shown on Figure 15(B), recovers the correct homotopy type of  $C \times L$ , which is the same as that of the base space  $C$ . Moreover, each fiber is a copy of  $L$  corresponding to a single vertex/cluster in the Mapper on Ball Mapper graph, consistent with contractibility of

the interval  $L$  was sampled from. Note that this is not always the case, as connected fibers may have nontrivial topology.

**5.3.2. Breast cancer dataset.** As a real-world application of the MoBM technique, we analyze the NKI breast cancer gene-expression dataset [39]. Such dataset has already been analyzed in a seminal Mapper paper [31] and can be downloaded from <https://data.world/deviramanan2016/nki-breast-cancer-data>. The data consist of the 1553 top varying genes for 272 breast cancer patients along with clinical metadata such as patient’s age, type of treatment and survival. Our goal is to build a Mapper graph that differentiates between subgroups of patients with different survival rates. The first attempt to construct a Ball Mapper over the whole data set using the correlation distance (since gene expressions are given as z-scores) fails to provide any information, see Figure 16. The same holds for BM graphs constructed using other metrics. In the next attempt we project the data to a 200-dimensional space using UMAP [28, 27]. The Ball Mapper graph obtained from the projected data using Euclidean distance can be found in Figure 16B. Finally, we pull this graph back to the original space using Mapper on Ball Mapper, thus obtaining the graph in Figure 16C. In particular, we are able to identify a distinct subgroup of 44 patients with 100% survival rate. While the detailed medical interpretation of such a finding is beyond the scope of this paper, the presented pipeline shows how methods introduced in this paper can be used in combination with other techniques to analyze noisy, high dimensional data.

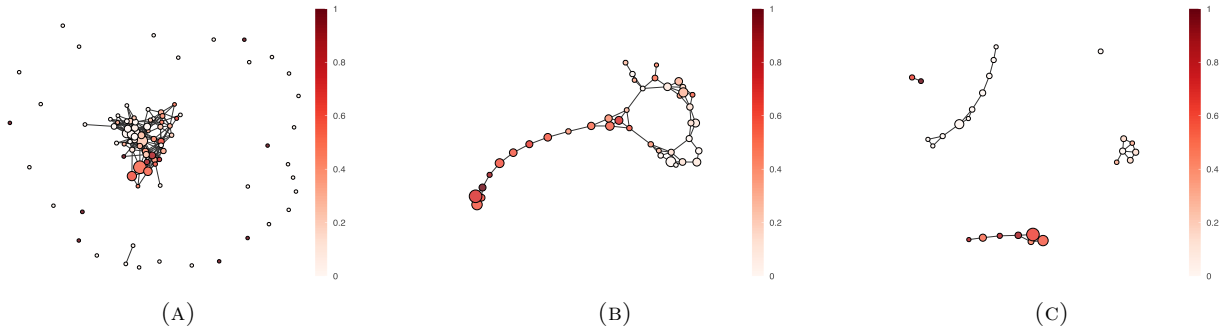


FIGURE 16. Three different Mapper-type graphs on the NKI dataset, nodes are colored by the fraction of patients who did not survive. Figure (A) depicts the Ball Mapper graph over the entire space, and it is not informative. Figure (B) depicts the Ball Mapper graph over a 200-dimensional projection obtained using UMAP. Figure (C) depicts the Mapper on Ball Mapper from Figure (B) to the original 1553-dimensional space. A clear separation between subgroups with different survival rates can be observed in Figure (C). In the last picture clusters containing only one or two elements have been removed for clarity.

## REFERENCES

- [1] James W Alexander. Topological invariants of knots and links. *Transactions of the American Mathematical Society*, 30(2):275–306, 1928.
- [2] Dror Bar-Natan, Scott Morrison, and et al. The Knot Atlas, 2011–2019. <http://katlas.org>.
- [3] Christopher M Bishop and Nasser M Nasrabadi. *Pattern recognition and machine learning*, volume 4. Springer, 2006.
- [4] Adam Brown, Omer Bobrowski, Elizabeth Munch, and Bei Wang. Probabilistic convergence and stability of random mapper graphs. *J. Appl. Comput. Topol.*, 5(1):99–140, 2021.

- [5] Benjamin A. Burton. The next 350 million knots. <http://regina-normal.github.io/data.html>, 2018. <http://regina-normal.github.io/data.html>.
- [6] Mathieu Carrière, Bertrand Michel, and Steve Oudot. Statistical analysis and parameter selection for mapper. *Journal of Machine Learning Research*, 19(12):1–39, 2018.
- [7] John H Conway. An enumeration of knots and links, and some of their algebraic properties. In *Computational problems in abstract algebra*, pages 329–358. Elsevier, 1970.
- [8] Alex Davies, Petar Veličković, Lars Buesing, Sam Blackwell, Daniel Zheng, Nenad Tomašev, Richard Tanburn, Peter Battaglia, Charles Blundell, András Juhász, et al. Advancing mathematics by guiding human intuition with ai. *Nature*, 600(7887):70–74, 2021.
- [9] Dheeru Dua and Casey Graff. Uci machine learning repository, 2017.
- [10] Paweł Dłotko, Davide Gurnari, and Radmila Sazdanovic. Mapper-type algorithms for complex data and relations - datasets and code, February 2023. <https://doi.org/10.5281/zenodo.7669610>.
- [11] Claus Ernst and DW Sumners. The growth of the number of prime knots. In *Mathematical Proceedings of the Cambridge Philosophical Society*, volume 102, pages 303–315. Cambridge University Press, 1987.
- [12] Martin Ester, Hans-Peter Kriegel, Jörg Sander, and Xiaowei Xu. A density-based algorithm for discovering clusters in large spatial databases with noise. KDD’96, page 226–231. AAAI Press, 1996.
- [13] Peter Freyd, David Yetter, Jim Hoste, WB Raymond Lickorish, Kenneth Millett, and Adrian Ocneanu. A new polynomial invariant of knots and links. *Bulletin (new series) of the American mathematical society*, 12(2):239–246, 1985.
- [14] Kam Hamidieh. A data-driven statistical model for predicting the critical temperature of a superconductor. *Computational Materials Science*, 154, 2018.
- [15] Jim Hoste. The enumeration and classification of knots and links. In *Handbook of knot theory*, pages 209–232. Elsevier, 2005.
- [16] Jim Hoste, Morwen Thistlethwaite, and Jeff Weeks. The first 1,701,936 knots. *The Mathematical Intelligencer*, 20(4):33–48, 1998.
- [17] Mark C Hughes. A neural network approach to predicting and computing knot invariants. *Journal of Knot Theory and Its Ramifications*, 29(03):2050005, 2020.
- [18] Slavik V Jablan and Sazdanovic Radmila. *LinKnot: knot theory by computer*, volume 21. World Scientific, 2007.
- [19] Vishnu Jejjala, Arjun Kar, and Onkar Parrikar. Deep learning the hyperbolic volume of a knot. *arXiv preprint arXiv:1902.05547*, 2019.
- [20] Vaughan F. R. Jones. A polynomial invariant for knots via von Neumann algebras. *Bull. Amer. Math. Soc. (N.S.)*, 12(1):103–111, 1985.
- [21] Louis H Kauffman and Laurence R Taylor. Signature of links. *Transactions of the American Mathematical Society*, 216:351–365, 1976.
- [22] Jesse SF Levitt, Mustafa Hajij, and Radmila Sazdanovic. Big data approaches to knot theory: Understanding the structure of the jones polynomial. *arXiv preprint arXiv:1912.10086*, 2019.
- [23] Lei Li, Wei-Yi Cheng, Benjamin S. Glicksberg, Omri Gottesman, Ronald Tamler, Rong Chen, Erwin P. Bottinger, and Joel T. Dudley. Identification of type 2 diabetes subgroups through topological analysis of patient similarity. *Science Translational Medicine*, 7:311ra174 – 311ra174, 2015.
- [24] WB Raymond Lickorish. *An introduction to knot theory*, volume 175. Springer Science & Business Media, 2012.
- [25] Charles Livingston. *Knot theory*, volume 24. Cambridge University Press, 1993.
- [26] Charles Livingston and Allison H. Moore. Knotinfo: Table of knot invariants. URL: [knotinfo.math.indiana.edu](http://knotinfo.math.indiana.edu), 09 2022.

- [27] L. McInnes, J. Healy, and J. Melville. UMAP: Uniform Manifold Approximation and Projection for Dimension Reduction. *ArXiv e-prints*, 2018.
- [28] Leland McInnes, John Healy, Nathaniel Saul, and Lukas Grossberger. Umap: Uniform manifold approximation and projection. *The Journal of Open Source Software*, 3(29):861, 2018.
- [29] Elizabeth Munch and Bei Wang. Convergence between categorical representations of reeb space and mapper. *SOCG*, 2016.
- [30] Nabil H. Mustafa. Computing Optimal Epsilon-Nets Is as Easy as Finding an Unhit Set. In Christel Baier, Ioannis Chatzigiannakis, Paola Flocchini, and Stefano Leonardi, editors, *46th International Colloquium on Automata, Languages, and Programming (ICALP 2019)*, volume 132 of *Leibniz International Proceedings in Informatics (LIPIcs)*, pages 87:1–87:12, Dagstuhl, Germany, 2019. Schloss Dagstuhl–Leibniz-Zentrum fuer Informatik.
- [31] Monica Nicolau, Arnold J. Levine, and Gunnar Carlsson. Topology based data analysis identifies a subgroup of breast cancers with a unique mutational profile and excellent survival. *Proceedings of the National Academy of Sciences*, 108(17):7265–7270, 2011.
- [32] Akira Ochiai. Zoogeographical studies on the soleoid fishes found in japan and its neighbouring regions-ii. *Bulletin of the Japanese Society of Scientific Fisheries*, 22, 1957.
- [33] Dłotko Paweł. Ball mapper: a shape summary for topological data analysis. *arXiv:1901.07410*, 2019.
- [34] Wanling Qiu, Simon Rudkin, and Paweł Dłotko. Refining understanding of corporate failure through a topological data analysis mapping of altman’s z-score model. *Expert Systems with Applications*, 156:113475, 2020.
- [35] Jacob Rasmussen. Khovanov homology and the slice genus. *Inventiones mathematicae*, 182(2):419–447, 2010.
- [36] G. Reeb. Sur les points singuliers d’une forme de pfaff complètement intégrable ou d’une fonction numérique. *C. R. Acad. Sci.*, 222:847–849, 1946.
- [37] Dale Rolfsen. *Knots and links*, volume 346. American Mathematical Soc., 2003.
- [38] Gurjeet Singh, Facundo Mémoli, Gunnar E Carlsson, et al. Topological methods for the analysis of high dimensional data sets and 3d object recognition. *PBG@ Eurographics*, 2, 2007.
- [39] Marc J. van de Vijver, Yudong D. He, Laura J. van’t Veer, Hongyue Dai, Augustinus A. M. Hart, Dorien W. Voskuil, George J. Schreiber, Johannes L. Peterse, Chris Roberts, Matthew J. Marton, Mark Parrish, Douwe Atsma, Anke Witteveen, Annuska Glas, Leonie Delahaye, Tony van der Velde, Harry Bartelink, Sjoerd Rodenhuis, Emiel T. Rutgers, Stephen H. Friend, and René Bernards. A gene-expression signature as a predictor of survival in breast cancer. *The New England Journal of Medicine*, 347(25):1999–2009, December 2002.
- [40] Matt Ward. Using neural networks to classify knots: Data mining and deep learning in knot theory. 2018.
- [41] Lee Y, Barthel SD, Dłotko P, Moosavi SM, Hess K, and Smit B. Quantifying similarity of pore-geometry in nanoporous materials. *Nat Commun.*, 2017.